Adv Polym Sci (2013) 252: 107–140
DOI: 10.1007/12_2012_173

Published online: 7 August 2012

Heterogeneous Dynamics of Polymer Thin Films as Studied by Neutron Scattering

Rintaro Inoue and Toshiji Kanaya

Abstract This review covers recent progress in studies on the dynamics of polymer thin films in the glassy state and near the glass transition temperature, as revealed by neutron scattering. First, the glassy dynamics including low energy excitation (Boson peak) and the fast localized process of polymer thin films at the picosecond timescale was studied to reveal the effect of film thickness. The dynamic heterogeneity of polymer thin films in the glassy state was also evaluated in terms of non-Gaussian parameters. Second, the glass transition temperature of polymer thin films was investigated using inelastic neutron scattering with high-energy resolution to clarify the mechanism of its dependence on film thickness. Finally, neutron reflectivity was used to study the distribution of glass transition temperature in a multilayered thin film consisting of deuterated polymer and hydrogenated polymer.

Keywords Dynamic heterogeneity · Inelastic and quasielastic neutron scattering · Polymer thin film

Contents

1 Introduction 108
2 Physical Properties of Polymer Thin Films 109
3 Basic Principles of Inelastic and Quasielastic Neutron Scattering 110
4 Glassy Dynamics of Polymer Thin Films in the Picosecond Region 113
5 Glass Transition of Polymer Thin Films in the Nanosecond Region 128
6 Distribution of Glass Transition Temperature in Thin Films 134
7 Concluding Remarks 137
References 138

R. Inoue and T. Kanaya (✉)
Institute for Chemical Research, Kyoto University, Uji, Kyoto-fu 611-0011, Japan
e-mail: kanaya@scl.kyoto-u.ac.jp

1 Introduction

Polymer thin films are utilized in the field of industrial applications such as lithography, coating, lubrication and so on and extensive studies have revealed that the thermal and mechanical properties of polymer thin films are quite different to those of bulk polymer [1, 2]. The thickness dependence of the glass transition temperature (T_g) [3–13], the thermal expansivity [7, 14], the ultra-slow expansion and contraction process [15], and the dewetting at temperatures lower than T_g of the bulk polymer [16, 17] are some of the representative examples of the anomalous properties of polymer thin films. At present, it is believed that most of singular physical properties of polymer thin films are related to the anomalous physical properties of the surface or interfacial region, hence we have to take into consideration the heterogeneous structure of polymer thin films to understand the singularity of polymer thin films.

For evaluation of the dynamic heterogeneity, there exist some experimental methods like nuclear magnetic resonance (NMR) [18], photo probe [19], and inelastic neutron scattering (INS) [20]. The advantage of INS is the direct probe of time (t) and space (Q) simultaneously; hence, we can discuss the heterogeneity of polymer thin films from both the static and dynamic point of view. Another advantage of INS is the relatively broad experimentally accessible temperature range, covering from far below bulk T_g to above bulk T_g. Hence, we can study the dynamics of polymer thin films in both glassy and molten state using INS. So far, few experimental approaches have been developed for studying the glassy state of polymer thin films even though some researchers have discussed the correlation between glassy dynamics and dynamics near T_g for bulk systems [21, 22]. We believe that glassy dynamics cannot be overlooked in the investigation of glass transition or related properties of polymer thin films, therefore measurements covering a broad temperature range are necessary.

In this review, we investigate the dynamic heterogeneity or anomalous dynamics of polymer thin films at temperatures from far below bulk T_g to above bulk T_g by neutron scattering. We also discuss the effect of dynamic heterogeneity on the resulting glassy and molten dynamics of polymer thin films.

The arrangement of this article is as follows: In Sect. 2, we briefly survey previous works on glass transition and related works on polymer thin films. Section 3 briefly describes the basic principles of inelastic and quasielastic neutron scattering for the reader's convenience. Section 4 discusses the thickness dependence of mean squared displacement $\langle u^2 \rangle$, as evaluated from Q^2 dependence of the elastic scattering intensity at the picosecond time scale. The physical origin for the change in $\langle u^2 \rangle$ with thickness is discussed from the point of view of molecular weight, Boson peak, and local relaxation (the so-called fast process). Afterwards, we discuss the dynamic heterogeneity of polymer thin films in terms of non-Gaussian parameters evaluated from the Q^2 dependence of elastic scattering intensity, taking advantage of the high Q accessible spectrometer. Section 5 is dedicated to the thickness dependence of T_g, as evaluated using ellipsometry and INS with different energy resolutions.

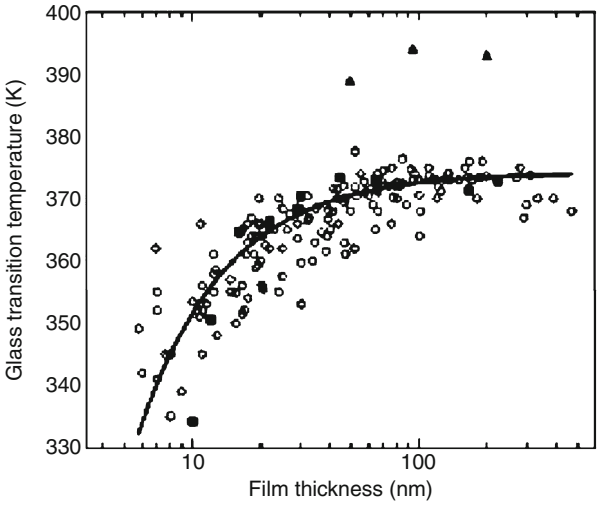

Fig. 1 Dependence of glass transition temperature on thickness of PS thin film supported on Si substrate Symbols other than *solid squares* were cited from formerly reported results and *solid squares* were from [5]. Solid line is the empirical fitting function to the observed data. For further detail please refer to [5]

The results are discussed with relation to the relaxation time map. The distribution of T_g in a thin film is discussed in Sect. 6 for multilayered thin films utilizing isotope labeling by neutron reflectivity. Concluding remarks are given in Sect. 7.

2 Physical Properties of Polymer Thin Films

In this section, we review recent investigations into the physical properties of polymer thin films. After the pioneering works by Keddie et al. [3], the thickness dependence of T_g was systematically studied by various methods including ellipsometry [3–5], X-ray/neutron reflectivity [6–8], dielectric relaxation [9, 10], local thermal analysis [11], and differential scanning calorimetry (DSC) [12, 13]. For example, the reduction in T_g with thickness was observed for polystyrene (PS) thin films supported on Si substrate, as shown in Fig. 1 [5]. The existence of a mobile surface layer with lower T_g than that of bulk polymer was directly confirmed by scanning probe microscopy (SPM) [23, 24]; hence, a two-layer model consisting of a mobile surface layer and internal bulk-like layer is often used to describe the thickness dependence of PS thin films. In the case of freely standing PS thin films, which have two air–polymer interfaces, a much more drastic reduction in T_g was reported by Forrest and coworkers [25, 26]. The reduction in T_g with decreasing film thickness was thought to be a universal feature of polymer thin films; however, this is not so. An increase in T_g with decreasing film thickness was observed for poly(methyl methacrylate) (PMMA) thin films supported on Si substrate with native oxide [3] due to strong interfacial interaction between the PMMA thin film and the Si substrate.

Singular physical properties of the surface or interfacial region of polymer thin films are not only observable from the thickness dependence of T_g but also from the other thermal properties of polymer thin films. A reduction in thermal expansivity with thickness reported by Miyazaki et al. [7] and DeMaggio et al. [14] is also related to the anomalous surface or interfacial properties of polymer thin films. In fact, DeMaggio et al. [14] used a three-layer model consisting of surface, bulk-like layer, and interfacial layer to describe the thickness dependence of thermal expansivity in the molten state, implying that both surface and interfacial effects cannot be ignored in describing the resulting physical properties of polymer thin films. Considering the so far reported results, a homogenous structure is no longer appropriate for the description of the physical properties of polymer thin films but instead a heterogeneous structure considering the singularity of surface or interfacial effects is necessary. If a heterogeneous structure were the real nature of polymer thin films, a distribution of physical properties including T_g in thin films would be expected, as pointed out by de Gennes [27] and Jones [28]. Experimentally, Torkelson et al. [29] first succeeded in evaluating the distribution of T_g in polymer thin films by fluorescence and multilayer methods and confirmed the existence of a distribution of T_g or a multilayered structure of T_g in thin films. Their results further reinforce the necessity to investigate the heterogeneous structure of polymer thin films.

Heterogeneity of polymer thin films was confirmed not only by static measurements but also from dynamic measurements. Fukao and Miyamoto [9] reported that the dielectric loss spectrum near T_g became broader with decreasing film thickness by dielectric relaxation. Kajiyama and coworkers [23, 24] used SPM to show that the apparent activation energy for the α_a-relaxation process at the surface region was smaller than that of bulk polymer near bulk T_g, implying a higher mobility at the surface region. Kim et al. [30] studied the surface dynamics near T_g by X-ray photon correlation spectroscopy (XPCS) and found that the acceleration of dynamics at the surface region was similar to that of bulk. These studies directly revealed the dynamic heterogeneity of polymer thin films; however, adequate experimental approaches are still lacking due to experimental difficulties. Further detailed and fruitful analyses from the perspective of the dynamic heterogeneity of polymer thin films are strongly desired and such approaches would offer better opportunities for understanding the unresolved problems of polymer thin films.

3 Basic Principles of Inelastic and Quasielastic Neutron Scattering

For better understanding of the present review, we include a brief account of the basic principles of inelastic and quasielastic scattering. For more detailed information and equations, the reader is referred to other books [31, 32].

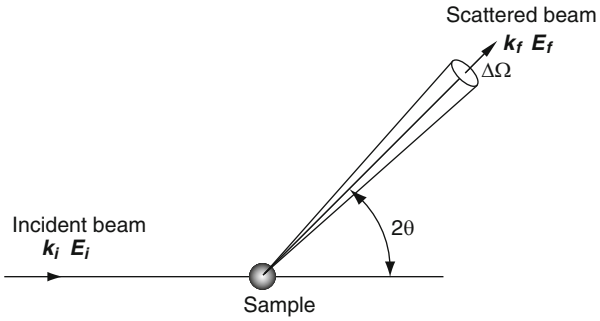

Fig. 2 Schematic view of the neutron scattering process. See text for details

In the case of inelastic or quasielastic scattering, the observable parameter is the double differential scattering cross-section $d^2\sigma/d\Omega dE$, which is the probability that an incident neutron with wave vector k_i and energy E_i is scattered by 2θ into a solid angle $d\Omega$ and with neutron energy in the range dE, as indicated in Fig. 2. The double differential scattering cross-section is related to the dynamic scattering:

$$\frac{\partial^2\sigma}{\partial\Omega\,\partial E} = \frac{1}{4\pi}\frac{k_f}{k_i}N[\sigma_{inc}S_{inc}(\boldsymbol{Q},\omega) + \sigma_{coh}S_{coh}(\boldsymbol{Q},\omega)], \tag{1}$$

where $\boldsymbol{Q}$ is the scattering vector, ω the neutron frequency, $S_{inc}(\boldsymbol{Q}, \omega)$ and $S_{coh}(\boldsymbol{Q}, \omega)$ are the incoherent and coherent scattering laws, σ_{inc} and σ_{coh} are the incoherent and coherent scattering cross-sections, and N is the number of atoms. The incoherent and coherent dynamic scattering laws are related to incoherent and coherent intermediate scattering functions $I_s(\boldsymbol{Q}, t)$ and $I(\boldsymbol{Q}, t)$, respectively, through the Fourier transformation:

$$S_{inc}(\boldsymbol{Q},\omega) = \frac{1}{2\pi}\int_{-\infty}^{\infty} I_s(\boldsymbol{Q},t)\,\exp(-i\omega t)\,dt, \tag{2}$$

$$S_{coh}(\boldsymbol{Q},\omega) = \frac{1}{2\pi}\int_{-\infty}^{\infty} I(\boldsymbol{Q},t)\,\exp(-i\omega t)\,dt. \tag{3}$$

$I_s(\boldsymbol{Q}, t)$ and $I(\boldsymbol{Q}, t)$ are defined by following equations:

$$I_s(\boldsymbol{Q},t) = \frac{1}{N}\sum_k \langle\exp\{-i\boldsymbol{Q}\boldsymbol{r}_k(0)\}\exp\{i\boldsymbol{Q}\boldsymbol{r}_k(t)\}\rangle, \tag{4}$$

$$I(\boldsymbol{Q},t) = \frac{1}{N}\sum_k\sum_l \langle\exp\{-i\boldsymbol{Q}\boldsymbol{r}_k(0)\}\exp\{i\boldsymbol{Q}\boldsymbol{r}_l(t)\}\rangle. \tag{5}$$

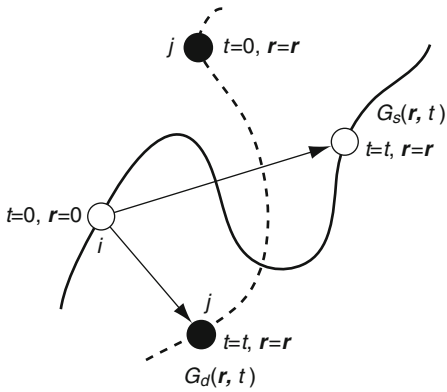

Fig. 3 Schematic view of Van Hove correlation functions. See text for details

Furthermore, incoherent and coherent dynamic scattering laws $S_{\mathrm{inc}}(\boldsymbol{Q}, \omega)$ and $S_{\mathrm{coh}}(\boldsymbol{Q}, \omega)$ are described by the time–space Fourier transformations of the time–space self- and pair-correlation functions $G_{\mathrm{s}}(\boldsymbol{r}, t)$ and $G(\boldsymbol{r}, t)$:

$$S_{\mathrm{inc}}(\mathbf{Q},\omega) = \frac{1}{2\pi}\int_{-\infty}^{\infty}\int_{0}^{\infty} \mathrm{d}\boldsymbol{r}\,\mathrm{d}t\, G_{\mathrm{s}}(\boldsymbol{r},t)\,\exp[\mathrm{i}(\boldsymbol{Q}\boldsymbol{r}-\omega t)], \tag{6}$$

$$S_{\mathrm{coh}}(\boldsymbol{Q},\omega) = \frac{1}{2\pi}\int_{-\infty}^{\infty}\int_{0}^{\infty} \mathrm{d}\boldsymbol{r}\,\mathrm{d}t\, G(\boldsymbol{r},t)\,\exp[\mathrm{i}(\boldsymbol{Q}\boldsymbol{r}-\omega t)]. \tag{7}$$

We also need to remark that the Van Hove correlation function $G_{\mathrm{d}}(\boldsymbol{r}, t)$ is used in the analysis of inelastic neutron scattering from liquids and is defined by:

$$G(\boldsymbol{r},t) = G_{\mathrm{s}}(\boldsymbol{r},t) + G_{\mathrm{d}}(\boldsymbol{r},t) \tag{8}$$

and is called the distinct correlation function. Assuming that a particle exists at position $\boldsymbol{r} = 0$ at time $t = 0$, then $G_{\mathrm{s}}(\boldsymbol{r}, t)$ gives the probability of finding the same particle in an interval $\mathrm{d}\boldsymbol{r}$ at $\boldsymbol{r}$ and at $t = t$. $G_{\mathrm{d}}(\boldsymbol{r}, t)$ is the probability of finding another particle in an interval $\mathrm{d}\boldsymbol{r}$ at $\boldsymbol{r}$ and at $t = t$. The physical meaning of $G_{\mathrm{d}}(\boldsymbol{r}, t)$ and $G_{\mathrm{s}}(\boldsymbol{r}, t)$ is schematically depicted in Fig. 3.

If the distribution of particle displacements $[r_k(t) - r_k(0)$ or $r_k(t) - r_l(0)]$ are described by a Gaussian distribution, then the incoherent and coherent intermediate scattering functions can be written, respectively, in terms of Q^2 only as:

$$I_{\mathrm{s}}(\boldsymbol{Q},t) = \frac{1}{N}\sum_{k}\exp\left\{-\frac{Q^2}{6}\left\langle\left(\left(r_k(t)-r_k(0)\right)^2\right\rangle\right\}, \tag{9}$$

$$I(\boldsymbol{Q},t) = \frac{1}{N}\sum_{k}\sum_{l}\exp\left\{-\frac{Q^2}{6}\left\langle\left(\left(r_k(t)-r_l(0)\right)^2\right\rangle\right\}. \tag{10}$$

The time-dependent mean square displacement can be obtained from the incoherent scattering measurements. It is also pointed out that the frequency-dependent mean square displacement can be obtained from the incoherent dynamic scattering law within the Gaussian approximation.

4 Glassy Dynamics of Polymer Thin Films in the Picosecond Region

In this section, we focus on glassy dynamics in the millielectronvolt (meV) or picosecond region including low energy excitation, which is responsible for the excess heat capacity of amorphous solids at 10–30 K [33–35], and the picosecond localized relaxation process, the "fast process" [36–38], in polymer thin films. Inelastic and quasielastic neutron scattering were used in order to understand the effect of heterogeneous structure on these localized glassy dynamics. The dynamic heterogeneity of polymer thin films in terms of non-Gaussian parameters [20, 39] was also studied utilizing a high Q accessible chopper spectrometer.

Before discusssing the details of dynamics from inelastic and quasielastic neutron scattering from polymer thin films, examples are given of the observed dynamic scattering law $S(Q, \omega)$ of PS thin films with thicknesses of 1,000 and 400 Å at temperatures from 11 to 408 K (Fig. 4a, b). A broad inelastic peak, the low energy excitation or so-called Boson peak, which is characteristic of amorphous systems, was observed at around 1.5 meV at temperatures lower than 200 K. With increasing temperature, the shape of the spectrum changed from inealstic-like to quasielastic-like, implying the onset of a relaxation process or anharmonic motion.

First we analyzed the elastic scattering intensity $I_{el}(Q)$ to evaluate the mean square displacement $\langle u^2 \rangle$. $\langle u^2 \rangle$ can be evaluated from the Q^2 dependence of incoherent elastic scattering intensity through $I_{el}(Q) = \exp[-\langle u^2 \rangle Q^2]$. The temperature dependence of evaluated $\langle u^2 \rangle$ is shown in Fig. 5 for the bulk polymer and for thin films with a thickness of 1,000 and 400 Å. $\langle u^2 \rangle$ is almost proportional to temperature T in the temperature range below 200 K, implying that the dynamics are mainly dominated by harmonic motion. With increasing temperature, $\langle u^2 \rangle$ began to deviate from a linear relationship and showed an extra anharmonic contribution. The examined temperature range covered the bulk T_g, but we could not detect the corresponding anharmonic contribution or excess increase at around bulk T_g, even for bulk sample. This implies that the energy resolution used ($\delta E \sim 0.20$ meV) was not enough to detect glass transition or α process [40]. The results from high-energy resolution measurements will be given in Sect. 5. The most important point from Fig. 5 is that $\langle u^2 \rangle$ decreased with the film thickness within the temperature range examined, indicating that the molecular mobility decreased with thickness.

Two possible reasons for the decrease in $\langle u^2 \rangle$ with thickness were considered. The first reason is the hardening due to polymer chain confinement in a thin film.

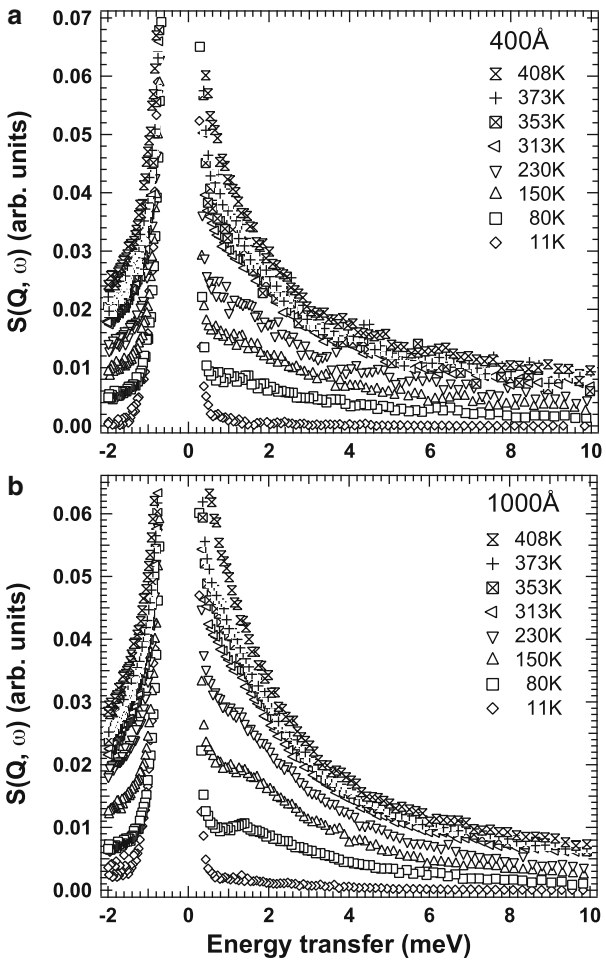

Fig. 4 Dynamic scattering law $S(Q, \omega)$ of PS thin films of thickness (**a**) 400 Å and (**b**) 1,000 Å at various temperatures, as indicated

In a thin film below polymer coil size, which can be represented by twice the radius of gyration ($2R_g$) [41], the polymer chains cannot sustain the normal coil form and deformation of the coil would occur as shown in Fig. 6a. Small angle neutron scattering (SANS) studies revealed that polymer chain conformation in thin films was different to that in bulk states [42, 43]. Such deformed polymer chains would have higher restoring force than that of a normal coil, resulting in the decrease in chain mobility with thickness. A second reason for the decrease in $\langle u^2 \rangle$ with thickness is the existence of a hard layer or low mobility layer [14], which would exist at the interface between the polymer thin film and the substrate (Fig. 6b). With decreasing film thickness, the fraction of such hard layer becomes large, under the assumption that the thickness of the hard layer is independent of the total film thickness.Which is the main reason for the decrease in $\langle u^2 \rangle$ with decreasing film thickness? In order to answer this problem, PS thin films with the same film

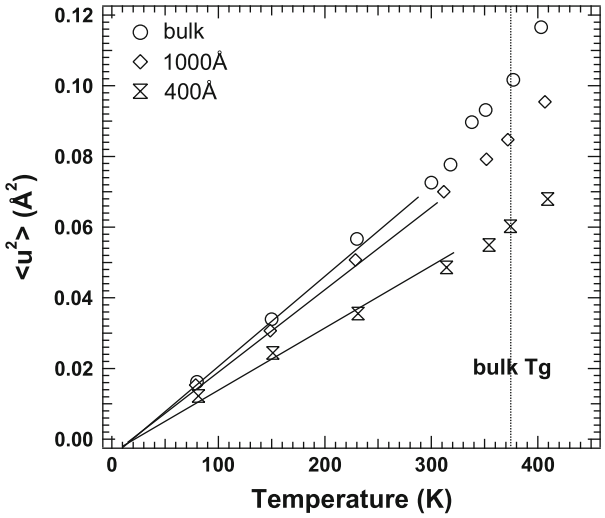

Fig. 5 Temperature dependence of mean square displacement $\langle u^2 \rangle$ for bulk PS and thin films of 1,000 and 400 Å

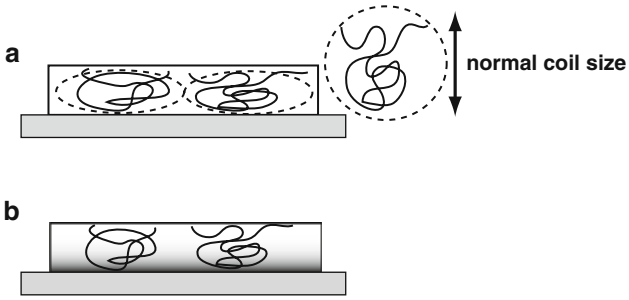

Fig. 6 Molecular pictures illustrating the reduction in mobility with thickness: (**a**) deformation of polymer chain and (**b**) hard layer at the interface

thickness for different molecular weight (M_w) were prepared, giving different ratios of the film thickness (d) to $2R_g$. If the confinement effect were dominant, a decrease in $\langle u^2 \rangle$ would be expected with the decrease in $d/2R_g$ because changing the ratio $d/2R_g$ means the changing of degree of confinement. If the interfacial effect were dominant, $\langle u^2 \rangle$ would be constant regardless of the ratio $d/2R_g$ (within experimental error) because the ratio of the interfacial layer to total film thickness is constant. Investigating the dependence of $\langle u^2 \rangle$ on M_w would offer a direct clue as to whether a homogenous structure (confinement effect) or a heterogeneous structure (interfacial effect) was reasonable. The temperature dependence of evaluated $\langle u^2 \rangle$ for different M_w is shown in Fig. 7. Evaluated values of $\langle u^2 \rangle$ for different M_w lie on a straight line

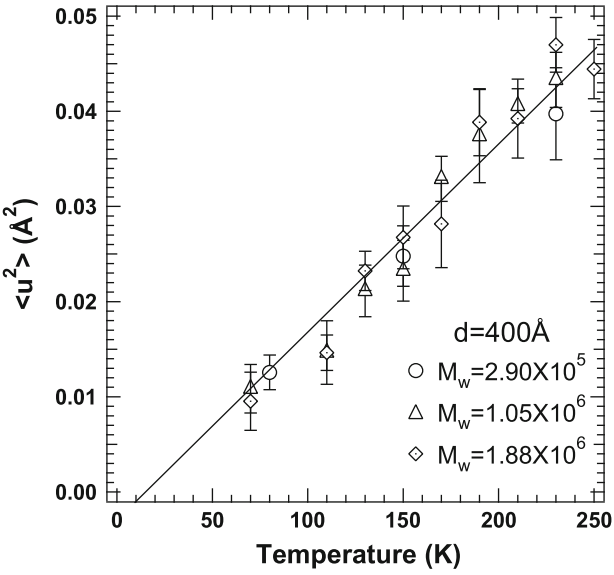

Fig. 7 Temperature dependence of mean square displacement $\langle u^2 \rangle$ for 400 Å films of PS of different molecular weights

within experimental error, implying that $\langle u^2 \rangle$ for a thin film of 400 Å thickness is independent of M_w in the temperature range examined. In order to check the validity of our assumption, $\langle u^2 \rangle$ was measured as a function of $d/2R_g$ and thickness d (Fig. 8). It was found that $\langle u^2 \rangle$ is only scaled by d, not $d/2R_g$, within the accuracy in the measurements. The procedure directly confirms that change of $\langle u^2 \rangle$ with thickness is not dominated by deformation of the polymer coil but by an interfacial hard or low mobility layer. Hence, a heterogeneous structure seems to be suitable for explaining the dynamics of polymer thin films as revealed by INS.

The hard interfacial layer seems to be the physical reason for the decrease in $\langle u^2 \rangle$ with decreasing thickness, as evaluated from elastic scattering. However, we do not know the effect of the hard interfacial layer or heterogeneous structure on the resulting inelastic and quasielastic neutron scattering. As a next step, inelastic and quasielastic neutron scattering from polymer thin films was studied to understand the physical origin of the decrease in $\langle u^2 \rangle$ with thickness. The observed $S(Q, \omega)$ was converted to the density of phonon states $G(\omega)$ [44] and the evaluated $G(\omega)/\omega^2$ values are shown in Fig. 9 for bulk polymer and thin films. A reduction in $G(\omega)$ with thickness was observed in the energy region 1–10 meV, suggesting that a decrease in $\langle u^2 \rangle$ with thickness was responsible for the decrease in $G(\omega)$ because $\langle u^2 \rangle$ is related to $G(\omega)$ through the relation [44]:

$$\langle u^2 \rangle = \frac{3\hbar}{2M} \int_0^\infty \frac{1}{\omega} \coth\left[\frac{\hbar\omega}{2k_B T}\right] G(\omega)\, d\omega. \tag{11}$$

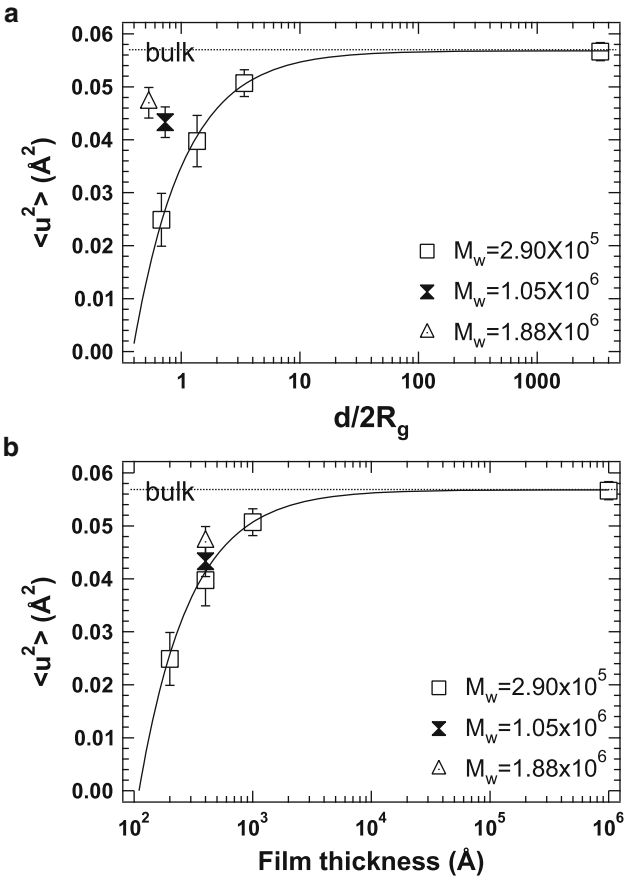

Fig. 8 (**a**) $\langle u^2 \rangle$ as a function of the ratio of film thickness to twice the radius of gyration ($d/2R_g$) for PS of different molecular weights. (**b**) $\langle u^2 \rangle$ as a function of film thickness (d) for PS of different molecular weights

The thickness dependence of the calculated $\langle u^2 \rangle$ from $G(\omega)$ and the elastic scattering are also plotted in Fig. 10. A consistency was found between $\langle u^2 \rangle$ from elastic scattering and that from inelastic scattering, supporting the proper background correction for the observed inelastic scattering from polymer thin films.

In the energy region examined, there exist at least two modes. One is a localized mode (Boson peak mode) and the other is an extended mode (Debye mode). The decoupling of both modes is needed to understand which mode contributes to the decrease in $G(\omega)$ with thickness in the energy region below 10 meV. The contribution of the Debye mode in $G(\omega)$ was evaluated from the Debye frequency ω_D and the contribution from the Boson peak mode was obtained by subtracting the Debye contribution from the total $G(\omega)$ [45]. For the thin films, the Debye contributions were estimated assuming that the amplitude of Debye mode and Boson peak mode are independent of film thickness. The Debye contribution from bulk and thin films

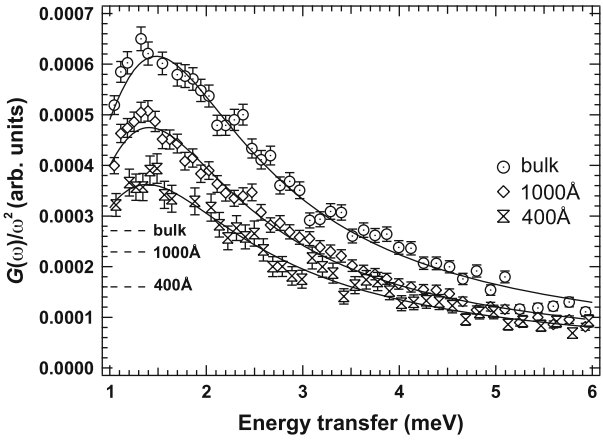

Fig. 9 Density of phonon states $G(\omega)$ divided by ω^2 for bulk PS and thin films of 1,000 and 400 Å; *dotted lines* show the Debye contribution

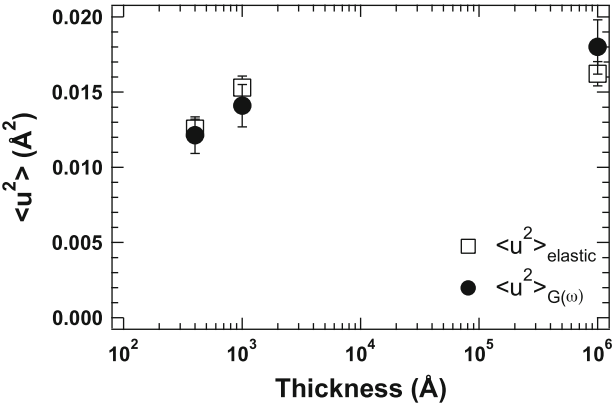

Fig. 10 Thickness dependence of $\langle u^2 \rangle$ as evaluated from Q^2 dependence of the elastic scattering intensity (*squares*) and $\langle u^2 \rangle$ as calculated from $G(\omega)$ at 80 K (*circles*)

are included in Fig. 9 as dashed lines, showing the significant depression of intensity in both Debye mode $G_D(\omega)$ and Boson peak mode $G_b(\omega)$. It implies that the decrease in $\langle u^2 \rangle$ with thickness could be attributed to the decrease in both the Debye mode and the Boson peak mode. As for the Boson peak, the peak position is independent of film thickness within experimental error. If we assume that peak energy is given by $\omega = \sqrt{f/m}$, where f is the harmonic force constant and m the effective mass, the present result implies that f is constant regardless of film thickness. That is to say, the effect of hardening on the Boson peak mode seems to be quite small. The physical origin of the decrease in intensity of both modes with decreasing film thickness must be considered independently.

The density of phonon states of Debye mode $G_D(\omega)$ is related to the average sound velocity v through the relation $G_D(\omega) = \frac{4\pi V\omega^2}{v^3}$, where V is the average atomic volume [46]. The reduction in $G_D(\omega)$ is the increase in sound velocity (v) due to the densification with decreasing film thickness. It was reported that polymer chains tend to form an ordered structure, exhibiting layering near the interface between thin film and the substrate [47, 48]. Gautam et al. [48] investigated the molecular structure of PS at the interface between polymer thin film and the substrate using IR–visible sum-frequency (SFG) spectroscopy and observed a preferred perpendicular orientation of the phenyl group with respect to the surface normal, indicating the in-plane orientation of the main chain at the interface between polymer thin film and substrate. The density of the layer at the interface must become larger due to such an ordered structure, resulting in an increase in v with decreasing film thickness. The ordered layer acts as a hard layer and results in a decrease in the Debye contribution $G_D(\omega)$.

As for Boson peak mode, earlier experimental results for bulk glass-formers offer useful information for the interpretation of our results. Inamura et al. [49] investigated the densification effect on Boson peak with SiO_2 glass and found that the intensity of the Boson peak decreased drastically just through the densification, as shown in Fig. 11a. For the polymer system, we [50] studied the effect of annealing on the Boson peak using PMMA bulk samples (Fig. 11b) and observed that Boson peak intensity decreased after annealing at 20 K below bulk T_g, without affecting the position of the Boson peak. Densification or annealing is a kind of structural change from the disordered state to the ordered state; hence, the physical origin of the Boson peak seems to be related to defects or voids or to structural disorder [51–53]. If there existed an ordered structure or hard interfacial layer at the interface between polymer thin film and substrate, it would result in a decrease in $G_b(\omega)$ with decreasing film thickness due to the high contribution from such an ordered layer. This situation results in a decrease in sites or voids for the Boson peak mode only, hence no shift of the Boson peak would be observed regardless of film thickness. The hard interfacial layer also seems to explain the decrease in both the Debye mode and the Boson peak mode and the idea of the existence of a hard layer is also applicable for the explanation of the thickness dependence of inelastic scattering behavior.

The observed dynamic scattering law $S(Q, \omega)$ was scaled by the Bose population factor after the correction for the Debye–Waller factor. The scaled spectra are shown in Fig. 12a for thin films with a thickness of 1,000 Å. The spectra were well scaled in the energy range at around 1.5 meV; on the other hand, excess scattering was observed below 1.5 meV with increasing temperature above about 200 K, suggesting the onset of the so-called fast process. The integrated scaled spectrum in the quasielastic region (0.70–1.5 meV) are plotted against temperature in Fig. 12b for the bulk polymer and for thin films of 1,000 and 400 Å. The temperature dependence of the integrated intensity for the 400 Å thin film is almost flat compared to those for the other film thicknesses in a low temperature region below ~230 K. The results suggest that the quasielastic scattering becomes more difficult in the thinner films. In order to study the characteristic features of the fast process in more detail, the model fit to the observed dynamic scattering law $S(Q, \omega)$ was performed and the following model function was employed for fitting [54]:

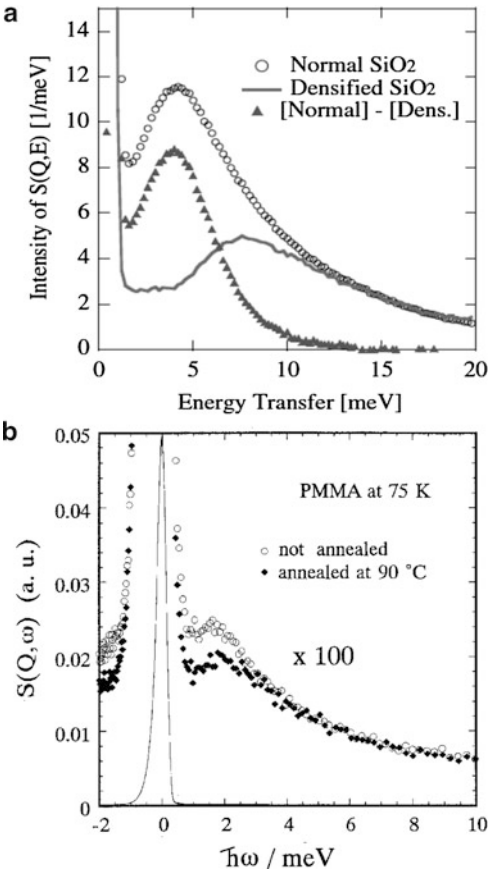

Fig. 11 (**a**) Dynamic scattering law $S(Q, \omega)$ of normal SiO_2 (*circles*) and densified SiO_2 (*solid line*) [49]. (**b**) Dynamic scattering law $S(Q, \omega)$ of PMMA, not annealed and annealed at 363 K [50]. The solid line corresponds to the observed full spectra and the solid symbols in (b) correspond to magnified sepctra with the scale factor of 100 ($\times 100$). PMMA at 75 K means $S(Q, \omega)$ of PMMA measured at 75 K

$$S(Q,\omega) = C(Q)[\{1 - A_{\text{fast}}(Q)\}\delta(\omega) + A_{\text{fast}}(Q)L(\Gamma,\omega)] + B(Q), \qquad (12)$$

where $A_{\text{fast}}(Q)$ is a fraction of the fast process, and $\delta(\omega)$ and $L(\Gamma, \omega)$ are a δ-function and a Lorentzian with half-width at half-maximum (HWHM) Γ, respectively. $C(Q)$ and $B(Q)$ are constants representing the Debye–Waller factor and inelastic flat background, respectively. The results of the fits for the 1,000 and 400 Å films at 408 K are shown in Fig. 13 and the observed spectra were well fitted with Eq. (12). The logarithms of the relaxation rate Γ and the fraction $A_{\text{fast}}(Q)$ are plotted against inverse of T in Fig. 14 for the bulk polymer and the 1,000 and 400 Å films. We found that Γ was more or less independent of film thickness, indicating that dynamics were not affected by film thickness. The most important point in Fig. 14 is that the fraction $A_{\text{fast}}(Q)$ decreased with the film thickness, and a similar decrease in intensity with the decrease in film thickness was also observed for the Boson peak. Comparing the thickness dependence of intensity or other properties like relaxation time, Boson peak intensity and the fast process is a fascinating approach for understanding the correlation between the fast process and Boson peak

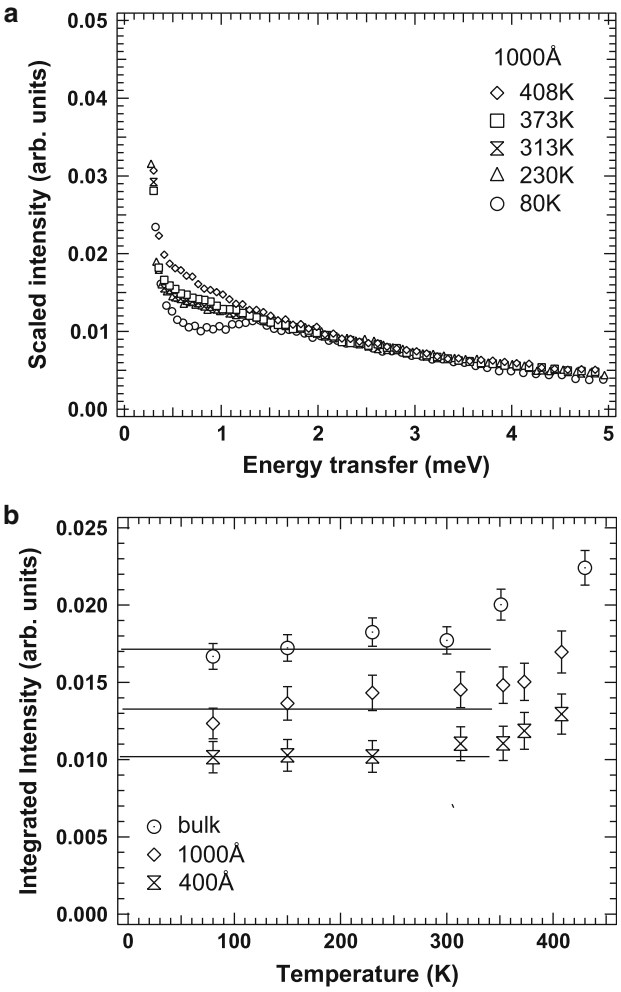

Fig. 12 (**a**) Bose-scaled inelastic scattering intensity at different temperatures after correcting for the Debye–Waller factor for PS thin films with a thickness of 1,000 Å. (**b**) Temperature dependence of integrated intensity of the Bose-scaled spectra in the energy range of 0.70–1.5 meV for bulk PS and thin films of 1,000 and 400 Å

in thin films. The thickness dependence of $G_b(\omega)$ and $A_{fast}(Q)$, which were normalized by those for bulk sample, and the thickness dependence of Γ and peak position of the Boson peak are plotted in Fig. 15. The thickness dependence of $G_b(\omega)$ and $A_{fast}(Q)$ are quite similar. Both the relaxation rate Γ of the fast process and the characteristic energy of the Boson peak are close to each other and are independent of the film thickness, indicating that the physical origin of the Boson peak and fast process are the same. From the thickness dependence of the Boson

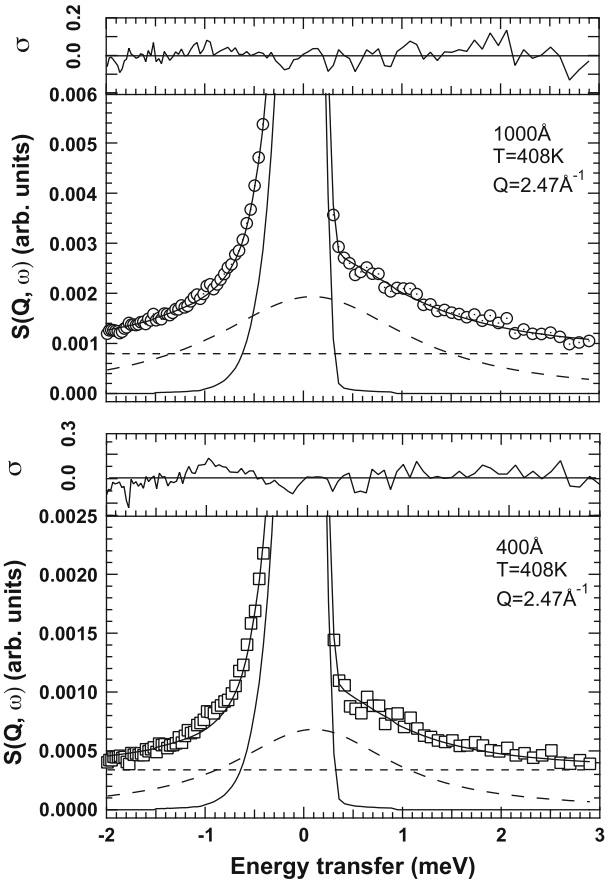

Fig. 13 Results of curve fit with Eq. (12) to the spectra of (**a**) 1,000 Å and (**b**) 400 Å thin PS films measured at a temperature of 408 K. The solid lines, which are overlapped the solid symbols are the results of curve fit with (12) and the other solids line corresponds to resolution function. (------) and (- - - - -) corresponds to flat background and lorentzian, respectively

peak mode, we suggest that the decrease in $G_b(\omega)$ is caused by the existence of hard interfacial layer; hence, a reduction in the fraction of fast process can also be attributed to an oriented interfacial layer.

Through the thickness dependence of elastic, inelastic, and quasielastic scattering in the millielectronvolt (or picosecond) region, it was found that the fast picosecond dynamics of polymer thin films was not described by homogenous dynamics but by heterogeneous dynamics, which were attributed to the orientation of molecular chains at the interface between polymer thin film and substrate.

We found that the existence of a hard interfacial layer was indispensable for the description of decreased mobility of polymer thin films with film thickness, implying that the heterogeneous structure was more enhanced with decreasing film thickness. Elucidating the heterogeneous structure of polymer thin films quantitatively is

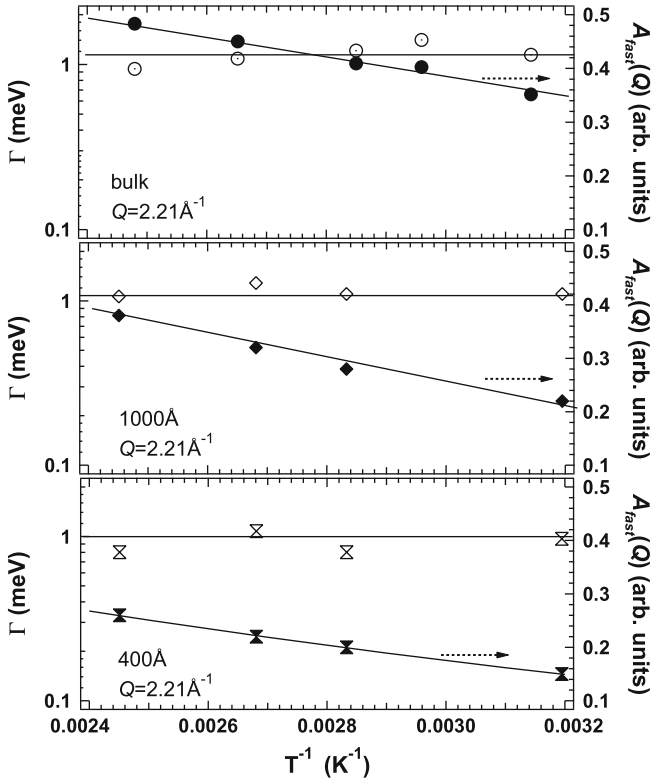

Fig. 14 Temperature dependence of relaxation rate Γ (*open symbols*) and fraction $A_{\text{fast}}(Q)$ of the fast process (*solid symbols*) for bulk PS and thin films of 1,000 and 400 Å

the target for understanding the unusual properties of thin films. The dynamic heterogeneity of polymer thin films in terms of the non-Gaussian parameter A_0 was then studied. In addition to the investigation on dynamic heterogeneity in thin films, we also studied the dynamic anisotropy; therefore, two scattering geometries (transmission and reflection geometries) were used, as shown in Fig. 16. In the transmission geometries the scattering vector Q is almost parallel and in reflection geometries it is perpendicular to the film surface; hence, the molecular motion parallel and perpendicular to the surface direction was studied. For the evaluation of dynamic anisotropy and heterogeneity, the Q dependence of $I_{\text{el}}(Q)$ must be evaluated.

Figure 17 indicates the Q^2 dependence of $I_{\text{el}}(Q)$ for the 1,000 and 200 Å films in the transmission and reflection geometries at 230 K, which were divided by $I_{\text{el}}(Q)$ at the lowest temperature. As seen in Fig. 17, $I_{\text{el}}(Q)$ cannot be described within the Gaussian approximation $I_{\text{el}}(Q) = \exp[-\langle u^2 \rangle Q^2]$, deviating in a high Q region above about 2.5 Å^{-1} due to higher order terms of Q. In order to describe the Q dependence of $I_{\text{el}}(Q)$ properly, higher order terms of Q must be taken into consideration. The non-Gaussian parameter was first introduced by Rhaman et al. [55]. According to

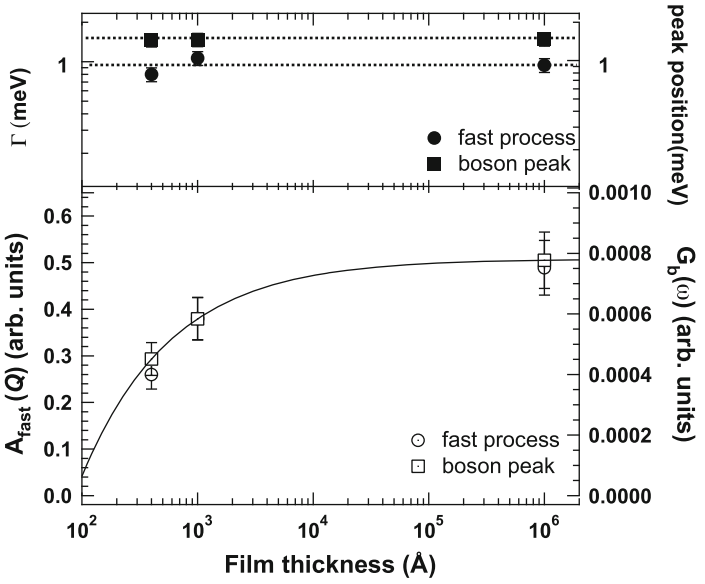

Fig. 15 Thickness dependence of the fraction of fast process $A_{\text{fast}}(Q)$ (*open circles*), relaxation rate Γ of fast process (*solid circles*), peak position of Boson peak (*solid squares*), and $G_{\text{b}}(\omega)$ (*open squares*)

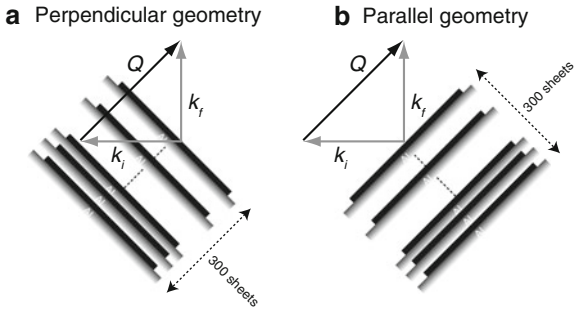

Fig. 16 Sample geometry for dynamic anisotropy measurements: (**a**) perpendicular (reflection) geometry and (**b**) parallel (transmission) geometry

them, the incoherent intermediate scattering function $I(Q, t)$ is obtained from the cumulant expansion up to the order of Q^4 as follows:

$$I(Q,t) = \exp\left(-\langle u^2\rangle(t)Q^2 + \frac{1}{2}A_0(t)[\langle u^2\rangle(t)]^2 Q^4\right). \tag{13}$$

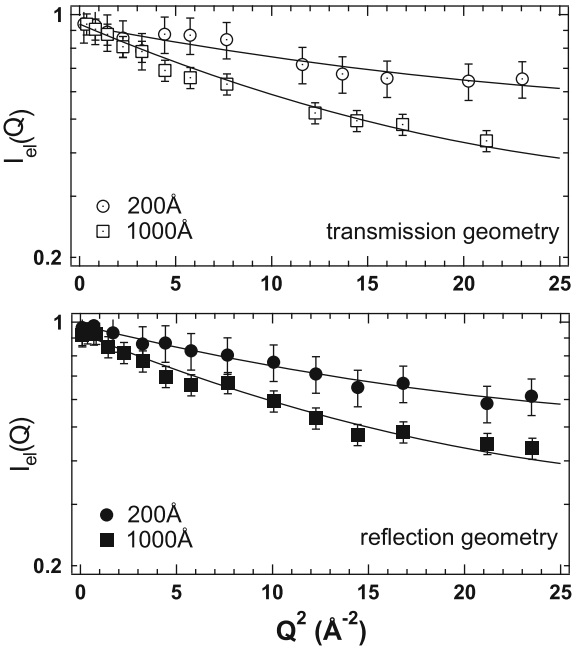

Fig. 17 Dependence of the elastic scattering intensity (I_{el}) on Q^2 for 1,000 and 200 Å thin PS films in transmission and reflection geometries at 230 K. The *solid lines* are results of fit with Eq. (19)

In this expression, the integrals of the velocity correlation functions, denoted by $\gamma_1(t)$ and $\gamma_2(t)$ [55], have been expressed in terms of the mean square displacement $\langle u^2 \rangle$. The non-Gaussian parameter $A_0(t)$ is given by the expression:

$$A_0(t) = \frac{3\langle u^4 \rangle(t)}{5[\langle u^2 \rangle(t)]^2} - 1. \tag{14}$$

It has been shown by Zorn [39] that the non-Gaussian parameter could be due to different phenomena such as dynamic heterogeneity, anharmonicity, and dynamic anisotropy. From the studies on several polymeric glass-formers, the most plausible origin of non-Gaussian parameter A_0 of the glass-forming materials was attributed to dynamic heterogeneity due to the difference in local environments [20, 39]. The dynamic heterogeneity must be a leading term in the non-Gaussian parameter for polymer thin films in the glassy state.

If the motion in the individual environment is Gaussian, the intermediate scattering function $I(Q, t)$ is given by:

$$I(Q,t) = \exp(-\langle u^2 \rangle Q^2). \tag{15}$$

It is further assumed that the mean square displacement has a distribution $g(\langle u^2 \rangle)$. For simplicity of calculation, Gaussian distribution was assumed as follows:

$$g(\langle u^2\rangle) = \frac{1}{\sqrt{2\pi\sigma^2}} \exp\left(-\frac{(\langle u^2\rangle - \overline{\langle u^2\rangle})^2}{2\sigma^2}\right), \tag{16}$$

where $\sigma^2 = \overline{(\Delta\langle u^2\rangle)^2} = \overline{(\langle u^2\rangle - \overline{\langle u^2\rangle})^2}$. The incoherent intermediate scattering function $I(Q, t)$ up to the order of Q^4 is obtained by averaging over the distribution:

$$I(Q,t) = \exp\left(-\overline{\langle u^2\rangle}Q^2 + \frac{A_0\overline{\langle u^2\rangle}^2}{2}Q^4\right), \tag{17}$$

where the non-Gaussian parameter A_0 is given by:

$$A_0 = \frac{\overline{\langle u^2\rangle^2} - \overline{\langle u^2\rangle}^2}{\overline{\langle u^2\rangle}^2}. \tag{18}$$

In this experiment, we observed dynamics in the frequency region; hence, the incoherent elastic scattering intensity of dynamic scattering law $S(Q, \omega = 0)$ is given by:

$$S(Q,\omega=0) = \exp\left(-\overline{\langle u^2\rangle}Q^2 + \frac{1}{2}A_0\overline{\langle u^2\rangle}^2Q^4\right), \tag{19}$$

where $\langle u^2\rangle$ is the mean square displacement in the frequency region. Equation (19) was applied to fit to the observed data in Fig. 17 and the results are shown by solid curves, giving good agreements. From the fits by Eq. (19), the mean square displacement $\overline{\langle u^2\rangle}$ and the non-Gaussian parameter A_0 were evaluated. The temperature dependence of $\overline{\langle u^2\rangle}$ and A_0 are summarized in Fig. 18. As the film thickness decreases, $\overline{\langle u^2\rangle}$ decreases, which is consistent with Figs. 5, 8, and 10. The non-Gaussian parameter A_0 increases with decreasing temperature and film thickness, showing that the dynamic heterogeneity increases with decreasing temperature and film thickness. By comparing the results from transmission and reflection geometries we can also discuss the dynamic anisotropy for thin films. No dynamic anisotropy was observed for 1,000 Å thin film; however, a slight difference in $\overline{\langle u^2\rangle}$ value was observed for the 200 Å thin film. The A_0 value in the transmission geometry is slightly larger than that in the reflection geometry for the 200 Å film, which must come from the anisotropic motion. As mentioned above, the dynamic anisotropy also contributes to the increase in A_0; however, the observed dynamic anisotropy only contributes to an increase in A_0, of ~0.05, implying that the contribution of dynamic anisotropy to A_0 is more or less negligible in the present study.

To observe the film thickness dependence of $\overline{\langle u^2\rangle}$ and A_0 quantitatively, $\overline{\langle u^2\rangle}$ and A_0 at 230 K were plotted as a function of film thickness (Fig. 19). As the film thickness decreases, the non-Gaussian parameter increases, implying that the dynamic heterogeneity increases with a reduction in film thickness. Our studies

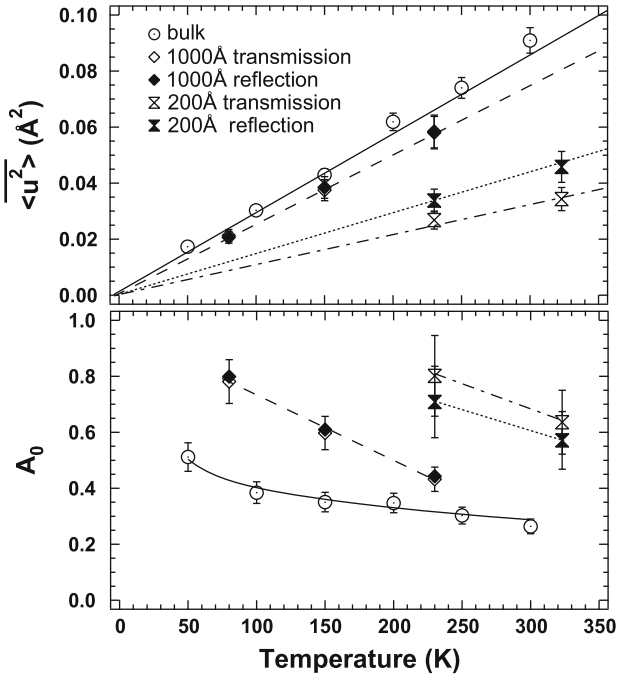

Fig. 18 Temperature dependence of mean square displacement $\langle u^2 \rangle$ and non-Gaussian parameter A_0 for bulk PS and thin films of 1,000 and 200 Å in transmission and reflection geometries

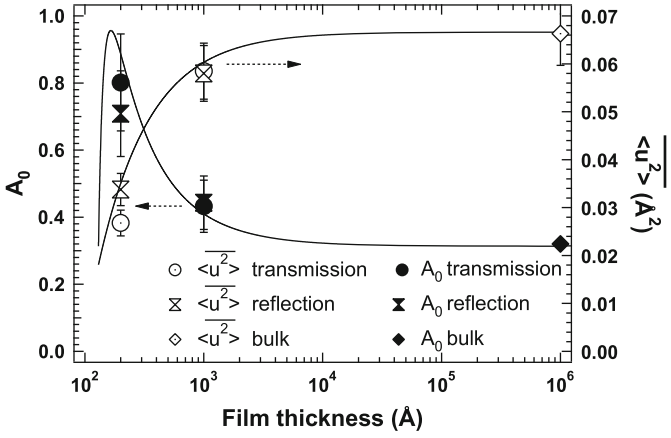

Fig. 19 Film thickness dependence of mean square displacement $\langle u^2 \rangle$ (*open symbols*) and non-Gaussian parameter A_0 (*solid symbols*) for bulk PS and thin films of 1,000 and 200 Å at 230 K

on the M_w dependence of $\langle u^2 \rangle$ have already shown that the interfacial layer is responsible for the decrease in $\langle u^2 \rangle$, therefore the increase in A_0 with decreasing film thickness reflects the multilayer structure of thin films or the existence of a hard interfacial layer. We tried to calculate A_0 as a function of film thickness based on a bilayer model, assuming that the thin film consists of a bulk-like layer and an interface hard layer. Under this assumption, $\overline{\langle u^2 \rangle}$ and $\overline{\langle u^2 \rangle}^2$ were calculated using Eqs. (20) and (21):

$$\overline{\langle u^2 \rangle} = \left(1 - \frac{\delta}{d}\right) \int \langle u^2 \rangle g(\langle u^2 \rangle)_{\text{bulk}} \, \mathrm{d}\langle u^2 \rangle + \frac{\delta}{d} \int \langle u^2 \rangle g(\langle u^2 \rangle)_{\text{dead}} \, \mathrm{d}\langle u^2 \rangle, \tag{20}$$

$$\overline{\langle u^2 \rangle}^2 = \left(1 - \frac{\delta}{d}\right) \int \langle u^2 \rangle^2 g(\langle u^2 \rangle)_{\text{bulk}} \, \mathrm{d}\langle u^2 \rangle + \frac{\delta}{d} \int \langle u^2 \rangle^2 g(\langle u^2 \rangle)_{\text{dead}} \, \mathrm{d}\langle u^2 \rangle, \tag{21}$$

where $d, \delta, g(\langle u^2 \rangle)_{\text{bulk}}$ and $g(\langle u^2 \rangle)_{\text{dead}}$ are the total thickness, the hard layer thickness, and distribution functions of $\langle u^2 \rangle$ in the bulk-like layer and in interfacial layer, respectively. The results of fit with a bilayer model are shown in Fig. 19 by solid curves, indicating that the bilayer model can describe the thickness dependence of observed A_0 and $\overline{\langle u^2 \rangle}$. In this calculation it was found that the thickness of the hard layer was ~130 Å and that $\overline{\langle u^2 \rangle}$ was ~0.018 Å^2 at 230 K. The value of $\overline{\langle u^2 \rangle}$ in the hard layer (~0.018 Å^2) at 230 K is very small compared with the bulk value (~0.066 Å^2).

The dynamic heterogeneity originating from a multilayer structure was evaluated based on the concept of non-Gaussian parameters. It was again confirmed that a heterogeneous dynamic structure was appropriate for the description of the dynamics of polymer thin films.

5 Glass Transition of Polymer Thin Films in the Nanosecond Region

In the previous section, the focus was on the glassy dynamics of polymer thin films and only the picosecond fast process was observed, even at temperatures above bulk T_g. The failure to detect the α process is due to a lack of energy resolution. We have studied the temperature dependence of $\langle u^2 \rangle$ with different energy resolutions, as shown in Fig. 20 [54]. In order to detect α processes properly, it seems that an energy resolution higher than about ~20 μeV is needed and such a high-energy resolution is possible with neutron backscattering [56] or neutron spin echo (NSE) [40]. In this section, we describe studies on the glass transition of polymer thin films using high-energy resolution spectrometry and ellipsometry.

The evaluated temperature dependence of $\langle u^2 \rangle$ with energy resolutions of 25 and 0.80 μeV for bulk PS and thin films with thicknesses of 1,000, 400 and 200 Å are shown in Fig. 21. $\langle u^2 \rangle$ decreased with decreasing film thickness in the temperature range examined and this tendency is consistent with the results from millelectronvolt

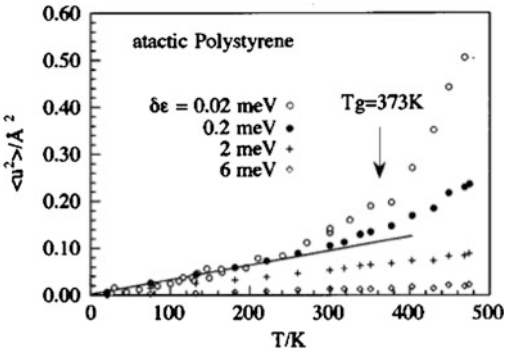

Fig. 20 Temperature dependence of $\langle u^2 \rangle$ of bulk PS for various energy resolutions [54]

(or picosecond) dynamics. In addition to the steep increase in $\langle u^2 \rangle$ due to the onset of the fast process at around 200 K, a drastic increase in $\langle u^2 \rangle$ was observed at around 370 K, which corresponds to the glass transition temperature in bulk ($T_g = 373$ K), suggesting detection of the α process [40, 56, 57]. This onset temperature of the α process was used as a determination of T_g by INS. The onset temperature of the α process shifted to higher temperature with decreasing film thickness, regardless of energy resolution. Ellipsometry measurements on PS thin films supported on Al-deposited Si substrates was also performed to realize similar substrate conditions as those used for INS measurements. The evaluated thickness dependence of T_g from ellipsometry and INS measurements are summarized in Fig. 22. It is evident that the thickness dependencies of T_g as measured by the two methods are completely contradictory. Similar contradiction in the thickness dependence of T_g has already been reported by Soles et al. [58, 59]. The authors observed a decrease in T_g with decreasing thickness for polycarbonate thin films from specular X-ray reflectivity (SXR) and positron annihilation lifetime spectroscopy (PALS) studies [58]. On the other hand, an increase in T_g with decreasing film thickness was observed from INS studies, as shown in Fig. 23. Furthermore, Soles et al. also studied the dynamics of several amorphous polymer thin films by INS and found that $\langle u^2 \rangle$ decreased and T_g increased with thickness for all the polymers investigated, regardless of the strength of interaction with substrates [59]. It seems that these anomalous phenomenon detected by INS might be related to certain aspects of polymer thin films.

Polymer thin film is a two-dimensionally confined system; hence, we would like to consider confined systems to find a plausible clue to the anomalous behavior. Schönhals et al. [60] studied the dynamics of glass-forming poly(methyl phenyl siloxane) (PMPS), which was confined to porous glass with a diameter in the nanometer range, using a combination of INS, dielectric relaxation, and temperature-modulated DSC to observe the anomalous dynamics compared to that of bulk polymer. The obtained relaxation time map for bulk PMPS and PMPS confined to nanoporous glass is shown in Fig. 24. For bulk PMPS, the temperature dependence of relaxation time was well described by the Vogel–Fulcher–Tammann (VFT) equation. On the other hand, the temperature dependence of relaxation time changed from a VFT equation to Arrhenius equation with a decrease in the diameter of the nanoporous

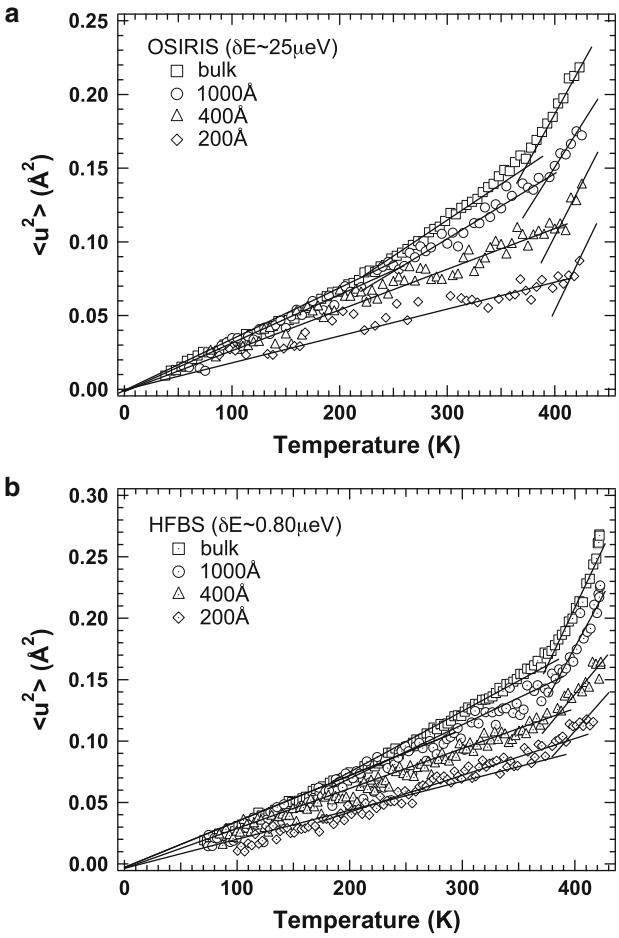

Fig. 21 Temperature dependence of $\langle u^2 \rangle$ of bulk PS and thin films of 1,000, 400, and 200 Å for δE of approximately (**a**) 25 μeV and (**b**) 0.80 μeV

glass, implying a decrease in activation energy with a reduction in pore size. Another interesting finding is that the relaxation times for bulk PMPS and other confined PMPS intersected at a certain temperature or frequency, which is here referred to as the "crossing point". Due to the existence of a crossing point in the relaxation time map, both acceleration and deceleration of dynamics were observable for PMPS confined to nanoporous glass compared to the bulk system. This implies that the contradiction dynamics was also possible for a confined PMPS system. Schönhals et al. discussed whether this change of dynamics by spatial confinement was attributed to the effect on a cooperatively rearranging region (CRR) [61]. For bulk glass-former, the size of CRR can extend adequately without any other spatial hindrance and the temperature dependence of relaxation time was described by a Vogel–Fulcher-type equation. With decreasing pore size, the glass-former cannot extend the CRR to the entire

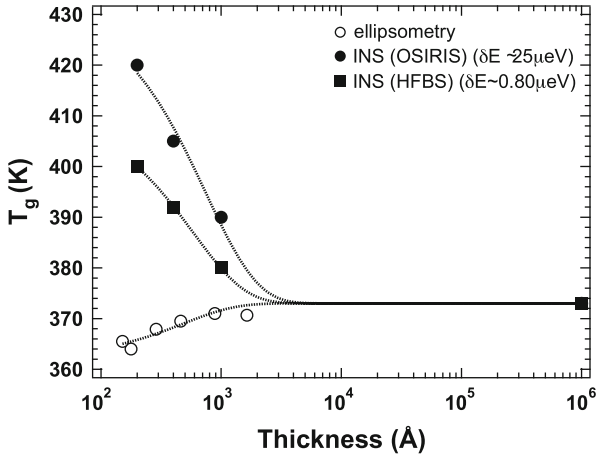

Fig. 22 Thickness dependence of T_g evaluated from INS with two different energy resolutions and by ellipsometry

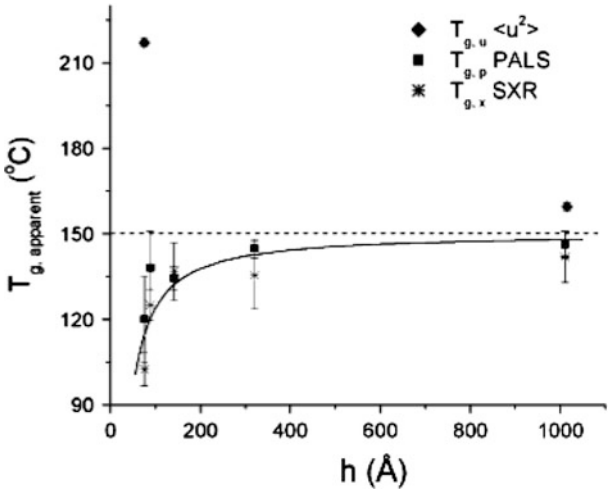

Fig. 23 Thickness (h) dependence of T_g evaluated from INS, PALS, and SXR of polycarbonate thin films [58]

system due to the limited pore diameter, resulting in the decrease in cooperativity or the onset of self-motion. The decrease in cooperativity means a decrease in activation energy; hence, a decrease in activation energy was observed with decreasing pore size. The above explanation is schematically summarized in Fig. 25.

Is the decrease in activation energy sufficient to realize the existence of a crossing point in the relaxation time map? If only the change of activation energy occurred, the crossing point in relaxation time map would be realized at extremely high temperature

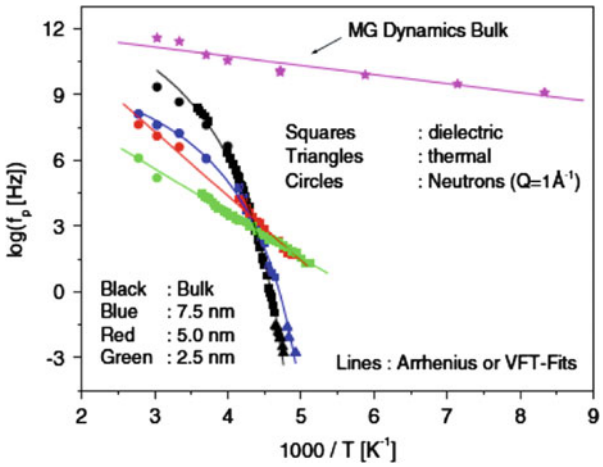

Fig. 24 Relaxation time map of bulk PMPS and PMPS films of different thicknesses confined to nanoporous glass, as observed with dielectric spectroscopy, thermal analysis, and INS [60]

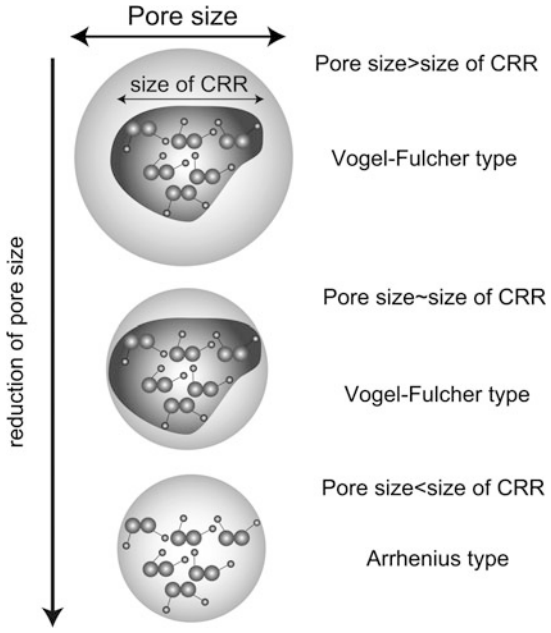

Fig. 25 Effect of spatial confinement on the cooperatively rearranging region (CRR)

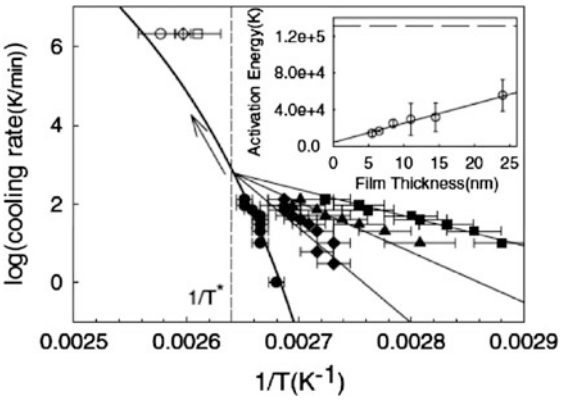

Fig. 26 The log(cooling rate) versus $1/T$ for PS thin films supported on Si substrate. *Inset* indicates the thickness dependence of activation energy [63]. Solid symbols represent PS thin films with different film thicknesses

or high frequency regions, which are not experimentally accessible. It is considered that the existence of an impenetrable wall would affect the resulting dynamics and, in fact, the dynamics of confined PMPS at a high frequency region was drastically slower than that of bulk polymer. These results imply that the segmental motion is strongly hindered by an effect of the wall surface, meaning a reduction in motional freedom. Both reduction in activation energy with decreasing pore size and a wall effect [62] are necessary to realize the anomalous dynamics observed for spatially confined glass-former.

Considering the analogy between the results of Schönhals et al. [60] and our results, the relaxation time map can serve as a supporting material for understanding our results. Hence, we tried to prepare a schematic relaxation time map for polymer thin films. As for the activation energy of thin films, Fakhraai and Forrest [63] investigated the thickness dependence of activation using ellipsometry with different cooling rates, as shown in Fig. 26, and found that the activation energy of the α process decreased at thicknesses below 61 nm. Interestingly, the temperature dependence of the relaxation rate was not described by a Vogel–Fulcher-type equation but by an Arrhenius type for the thinnest film investigated. Compared to the reported size of CRR for PS (~3 nm) [64, 65], the onset film thickness for the observation of a decrease in activation energy is quite large. The authors supposed that the rearrangement of cooperative dynamics at the free surface might be involved in the change in temperature dependence of relaxation time observed for a relatively thick PS thin film (~61 nm); however, more detailed experimental evidence is still needed to verify this idea.

The relaxation time map, which reflects the decrease in activation energy with thickness, and the crossing point are shown in Fig. 27. Utilizing the constructed relaxation time map, the contradictory results observed for the thickness dependence of T_g using two different methods can be explained. Assuming that the ellipsometry measurement detects T_g when relaxation time crosses a certain slow characteristic time (Fig. 27, line A), T_g must decrease with the film thickness. INS detects T_g at a relatively high frequency region compared to other methods and it is assumed that INS detects T_g at a frequency above the crossing point (Fig. 27, line B or line C). Under such conditions, T_g would increase with decreasing film thickness . As a result, both

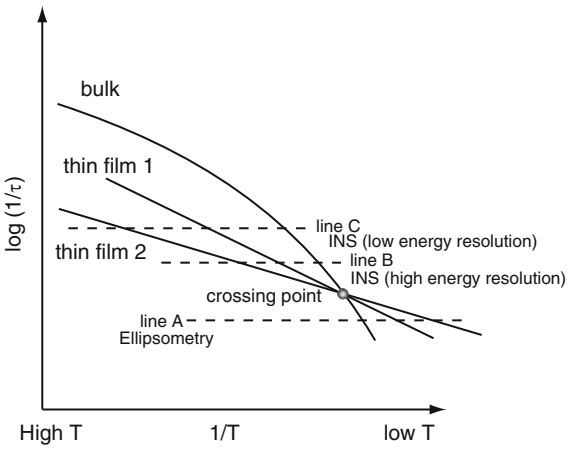

Fig. 27 Relaxation time map for PS thin films, used to explain the film thickness dependence of T_g. Thin film 2 is thinner than thin film 1. See text for full description

INS results and ellipsometry results seem to be explained using the schematic sketch of the relaxation time map. INS measurements with different energy resolutions can serve as a self-check for the relaxation time map, and an increase in T_g would be expected with lowering the energy resolution for same sample. Returning to Fig. 22, it was confirmed that T_g increased with lowering energy resolution; hence, the schematically prepared relaxation time map is consistent with our results.

In order to construct a more reliable relaxation time map quantitatively, complementary use of other methods like dielectric relaxation measurements and INS measurements with different energy resolutions are still needed.

6 Distribution of Glass Transition Temperature in Thin Films

In the previous section, it was supposed that the anomalous cooperative dynamics in thin films compared to that of bulk polymer is related to the singular glass transition behavior in thin films. In order to clarify the above idea, it is better to investigate the cooperative dynamics or CRR in thin films directly; however, concrete theoretical and experimental approaches have not been presented up to now. Evaluation of the distribution of T_g in thin films would be a good starting point for accomplishing such a difficult task.

One advantage of neutron scattering is that it can discern hydrogenated and deuterated molecules because of the difference in scattering length density, and this difference can serve as a kind of labeling. In this section, we describe the distribution of T_g in thin films using multilayered PS thin films consisting of deuterated polystyrene (d-PS) and hydrogenated polystyrene (h-PS) using neutron reflectivity.

The obtained neutron reflectivity profiles from d-PS/h-PS/d-PS three-layered thin films at several temperatures are shown in Fig. 28 and the reflectivity profiles were analyzed with the formula derived by Parratt [66]. The solid lines in Fig. 28

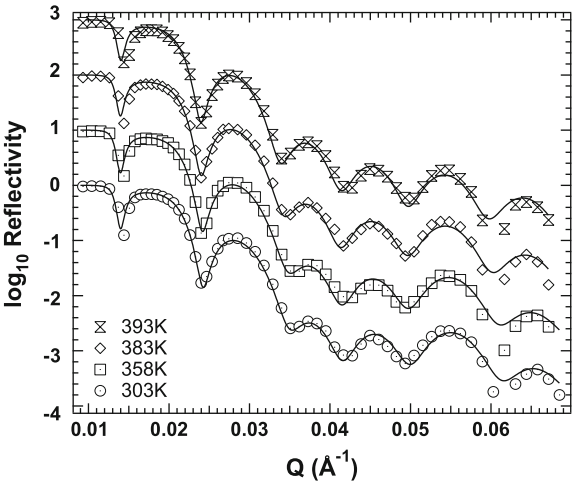

Fig. 28 Neutron reflectivity profiles from d-PS/h-PS/d-PS three-layered thin films at various temperatures. *Solid lines* correspond to the results of fit with a three-layered model

are the results of fits with the three-layer model. The agreements of fit were very good for the temperatures investigated, indicating that a three-layer model is appropriate for the description of our results at temperatures both above and below bulk T_g. The thermal expansivity and T_g of total film thickness was investigated as an initial step, and the temperature dependence of the total film thickness is given in Fig. 29. The evaluated T_g of the total thickness was 374 K and this value was almost the same as the bulk T_g (376 K) within experimental error. Furthermore, the thermal expansivity in the glassy and molten states were 9.4×10^{-5} and 4.9×10^{-4} K^{-1}, respectively, and these values were almost the same as the bulk thermal expansivity (1.1×10^{-4} and 5.1×10^{-4} K^{-1}). It was found that the total film thickness (~640 Å) exhibited bulk-like behavior and these results were consistent with those of Miyazaki and coworkers [7].

As a next step, the temperature dependence of the three different component layers was studied. The layers were named first layer, second layer, and third layer from the top to bottom, as shown in Fig. 29. Evaluated T_g of the first layer was 358 K, of the second layer 374 K, and was not detectable for the third layer within the experimental temperature range. The evaluated T_g from the first and second layers were consistent with the works by Ellison and Torkelson [29]. As for the interpretation of T_g near the interface between polymer thin film and substrate, the works by Tanaka et al. [67] are quite helpful. They authors observed about 20 K increase in T_g compared with that of bulk at a distance ~200 Å from the substrate for PS thin films supported on SiO_x substrate. The thickness of the bottom layer was ~150 Å; hence, at least a 20 K increase in T_g at the bottom layer would be expected. Considering the zero thermal expansivity of the bottom layer, the T_g of the interfacial layer had a high T_g and possibly shifted out of the experimentally accessible temperature range (above 403 K). Although the total film thickness exhibited a bulk-like behavior, each component layer showed different T_g, supporting the idea of dynamic heterogeneity in thin films as well as glassy dynamics.

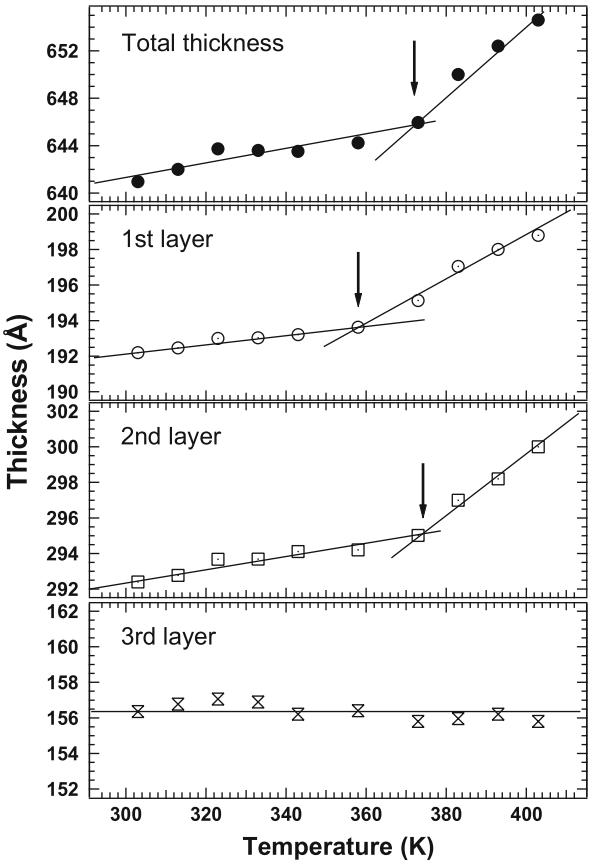

Fig. 29 Temperature dependence of the total film thickness and thickness of first, second and third layers for a three-layered thin film. The *arrows* indicate the evaluated T_g

Utilizing the results from multilayered thin film studies, we would like to understand one aspect of the singular physical properties of "single" PS thin films. Miyazaki et al. [7] reported a decrease in both T_g and thermal expansivity with decreasing PS film thickness using X-ray reflectivity. From the thickness dependence of T_g we get an impression of softening or enhancement of mobility with decreasing film thickness. On the other hand, from the thickness dependence of thermal expansivity we get an impression of hardening or decrease in mobility with decreasing film thickness. Seemingly, the thickness dependence of T_g is inconsistent with a thickness dependence of thermal expansivity despite being measured in the same PS thin films; however, we must try to understand Miyazaki's results. We have found that polymer thin films consist of a mobile surface layer, middle bulk-like layer, and interfacial layer. We have shown that T_g of the interfacial layer was too high to be detected in the present experimental range. As a result, only the T_g of the surface layer and bulk-like layer in polymer thin films can be detected in the experimental temperature range and the interfacial contribution can be neglected. This is the main reason why the two-layer model works for the description of the

thickness dependence of T_g of PS thin films, in spite of the existence of an interfacial layer [7]. That is to say, a decrease in T_g with decreasing film thickness is mainly responsible for the contribution of the surface layer or "surface effect."

How can we interpret the thickness dependence of thermal expansivity? In principle, the thermal expansivity of "total" thin film is given by the average of thermal expansivity of the surface layer, bulk-like layer, and interfacial layer:

$$\alpha = \frac{1}{D} \sum_{i=\text{surf,bl,int}} \alpha_i d_i, \quad D = \sum_{i=\text{surf,bl,int}} d_i, \tag{22}$$

where α, α_{surf}, α_{bl}, α_{int} are the thermal expansivity of total film thickness, surface layer, bulk-like layer and interfacial layer, respectively and D, d_{surf}, d_{bl}, d_{in} are the thickness of total film thickness, surface layer, bulk-like layer, and interfacial layer, respectively. From multilayered thin film studies we could not find a clear change in thermal expansivity of the surface layer (α_{surf}) and bulk-like layer (α_{bl}) compared with that of bulk (α_{bulk}); therefore, it is easily supposed that the surface effect alone is inadequate to understand the thickness dependence of thermal expansivity of polymer thin films. As for the thermal expansivity of the bottom or interfacial layer in a multilayered thin film, we observed zero or quite small thermal expansivity (see third layer in Fig. 29). With decreasing film thickness, the decrease in α might be due to a high contribution from the interfacial layer. Assuming the extreme case that a polymer thin film consists of surface layer and interfacial layer only, then the thermal expansivity would be given by $\alpha_{surf}d_{surf}/D$, resulting in the decrease in thermal expansivity with decreasing thickness. The "interfacial effect" is indispensable for the explanation of the thickness dependence of thermal expansivity of PS thin films.

Taking into consideration of both surface effect and interfacial effect we can understand the decrease in thermal expansivity and T_g with decreasing thickness observed simultaneously for the same PS thin film without inconsistency.

Through the multilayer thin film studies we could also clarify that the resulting physical properties of polymer thin films are directly determined by the balance or competition between the surface effect and interfacial effect.

7 Concluding Remarks

We have reviewed recent studies on the dynamics of polymer thin films using neutron scattering at temperatures ranging from far below bulk T_g to above bulk T_g and found that heterogeneity is the essential notion for understanding the physical properties of polymer thin films from the perspective of dynamics. If we want to grasp the essence of polymer thin films, we have to aim at investigating the dynamics at a selective position in a thin film (not in entire films), that is to say the distribution of dynamics in a thin film. Such an experimental approach is quite new at present; however, some researchers have started investigations.

Kim et al. studied only the surface region of a polymer thin film by changing the incident angle of X-rays using XPCS [30]. Multilayer methods are also useful and Torkeloson and coworkers used fluorescence to study the aging dynamics (glassy dynamics) of multilayered labeled PMMA thin films [68]. Thanks to the sophistication of neutron source devices, isotope labeling of multilayered thin films might be a reliable method for studying the distribution of dynamics in thin films by INS directly. Is there an alternative method for evaluating heterogeneous dynamics without resorting to labeling or multilayered methods? Pratt et al. [69] studied the dynamics of polymer thin films at different positions in a polymer thin film using slow muons with different incident energies. The advantage of their method is that the dynamics at the desired position in a thin film can be probed just by changing the incident muon energy, which corresponds to changing the interpenetration depth in the thin film. At present, the energy resolution or the width of interpenetration depth is very broad; hence, analyses such as the distribution of relaxation time along the depth direction are not yet practical. However, the refinement of instrumentation would offer better opportunities to study the distribution of dynamics at a given position in polymer thin films.

If we can succeed in evaluating the distribution of dynamics near T_g in thin films qualitatively, we have a chance to evaluate the distribution of CRR in thin films and can discuss the origin of anomalous dynamics in polymer thin films directly. For this purpose, new experimental methods and further theoretical approaches are indispensable.

References

1. Jones RL, Richards RW (1999) Polymers at surface and interfaces. Cambridge University Press, Cambridge
2. Karim A, Kumar S (eds) (2000) Polymers surfaces, interfaces and thin films. World Scientific, Singapore
3. Keddie JL, Jones RAL, Cory RA (1994) Faraday Discuss 98:219
4. Keddie JL, Jones RAL, Cory RA (1994) Europhys Lett 27:59
5. Kawana S, Jones RAL (2001) Phys Rev E 63:21501
6. Kanaya T, Miyazaki T, Watanabe H, Nishida K, Yamano H, Tasaki S, Bucknall DB (2003) Polymer 44:3769
7. Miyazaki T, Nishida K, Kanaya T (2004) Phys Rev E 69:061803
8. Orts WJ, van Zanten JH, Wu WL, Satija SK (1993) Phys Rev Lett 71:867
9. Fukao K, Miyamoto Y (2000) Phys Rev E 61:1743
10. Tress M, Erber M, Mapresa EU, Huth H, Müller J, Serghei A, Schick C, Eichhorn K-J, Voit B, Kremer F (2010) Macromolecules 43:9937
11. Fryer DS, Nealey PF, de Pablo JJ (2000) Macromolecules 33:6439
12. Efremov MY, Olson EA, Zhang M, Zhang Z, Allen LH (2004) Macromolecules 37:4607
13. Efremov MY, Olson EA, Zhang M, Zhang Z, Allen LH (2003) Phys Rev Lett 91:085703
14. DeMaggio DB, Frieze WE, Gidley DW, Zhu M, Hristov HA, Yee AF (1997) Phys Rev Lett 78:1524
15. Miyazaki T, Nishida K, Kanaya T (2004) Phys Rev E 69:022801
16. Reiter G (1993) Europhys Lett 23:579

17. Reiter G (1994) Macromolecules 27:4607
18. Schmit-Roht K, Spiess HW (1991) Phys Rev Lett 66:3020
19. Cicerone MT, Blackburn FR, Ediger MD (1995) J Chem Phys 102:471
20. Kanaya T, Tsukushi I, Kaji K (1997) Prog Theo Phys Suppl 126:133
21. Buchenau U, Zorn R (1992) Europhys Lett 18:523
22. Sokolov AP, Rossler E, Kisliuk A, Quitmann D (1993) Phys Rev Lett 71:2062
23. Kajiyama T, Tanaka K, Takahara A (1998) Polymer 39:4665
24. Tanaka K, Takahara A, Kajiyama T (2000) Macromolecules 33:7588
25. Forrest JA, Dalnoki-Veress K, Stevens JR, Duchter JR (1996) Phys Rev Lett 77:2002
26. Dalnoki-Veress K, Forrest JA, Murray C, Gigault C, Duchter JR (1996) Phys Rev E 63:31801
27. de Gennes PG (2000) Eur Phys J E 2:201
28. Jones RAL (2000) Eur Phys J E 2:205
29. Ellison CJ, Torkelson JM (2003) Nat Mater 2:695
30. Kim H, Rühm A, Lurio LB, Basu JK, Lal J, Lumma D, Mochrie SGJ, Shinha SK (2003) Phys Rev Lett 90:068302
31. Bée M (1988) Quasielastic neutron scattering, principles and applications in solid state chemistry, biology and materials science. Taylor & Francis, Bristol
32. Imae T, Kanaya T, Furusaka M, Torikai N (eds) (2011) Neutrons in soft matter. Wiley, Hoboken
33. Philips WA (ed) (1981) Amorphous solids – low temperature properties. Springer, Berlin
34. Buchenau U, Nücker N, Dianoux AJ (1984) Phys Rev Lett 53:2316
35. Frick B, Richter D (1993) Phys Rev B 47:795
36. Buchenau U, Schönfeld C, Richter D, Kanaya T, Kaji K, Wehrmann R (1994) Phys Rev Lett 73:2344
37. Fujara F, Petry W (1987) Europhys Lett 4:921
38. Kanaya T, Kawaguchi T, Kaji K (1993) J Chem Phys 98:8262
39. Zorn R (1997) Phys Rev B 61:6249
40. Richter D, Monkenbusch M, Arbe A, Colmenero J (2005) Adv Polym Sci 174:1
41. Brandrup J, Immergut EH, Grulke EA (eds) (1999) Polymer handbook, 4th edn. Wiley, New York
42. Kraus J, Müller-Buschbaum P, Kuhlmann T, Schubert DW, Stamm M (2000) Europhys Lett 49:210
43. Brulet A, Boue F, Menelle A, Cotton JP (2002) Macromolecules 35:8878
44. Marshall W, Lovesey SW (1971) Theory of thermal neutron scattering. Clarendon, Oxford
45. Inoue R, Kanaya T, Nishida K, Tsukushi I, Shibata K (2006) Phys Rev B 74:021801
46. Inoue K, Kanaya T, Ikeda S, Kaji K, Shibata K, Misawa M, Kiyanagi Y (1991) J Chem Phys 95:5333
47. Zhang JM, Zhang DH, Shen DY (2002) Macromolecules 35:5140
48. Gautam KS, Schwab AD, Dhinojwala A, Zhang D, Dougal SM, Yeganeh MS (2000) Phys Rev Lett 85:3854
49. Inamura Y, Arai M, Nakamura T, Otmo T, Kitamura N, Bennington SM, Hanon AC, Buchenau U (2001) J Non-Cryst Solids 293:389
50. Kanaya T, Kaji K (2001) Adv Polym Sci 154:87
51. Nakayama T (1998) Phys Rev Lett 80:1244
52. Das SP (1999) Phys Rev E 59:3870
53. Granato AV (1996) Physica B 220:270
54. Kanaya T, Kawaguchi T, Kaji K (1996) J Chem Phys 104:3841
55. Rahman A, Singwi KS, Sjölander A (1962) Phys Rev 126:986
56. Frick B, Buchenau U, Richter D (1995) Colloid Polym Sci 273:413
57. Arbe A, Colmenero J, Alvarez F, Monkenbusch M, Richter D, Farago B, Frick B (2003) Phys Rev E 67:051802
58. Soles CL, Douglas JF, Wu W, Peng H, Gidley DW (2004) Macromolecules 37:2890
59. Soles CL, Douglas JF, Wu W, Peng H, Gidley DW (2003) Macromolecules 36:373
60. Schönhals A, Goering H, Schick C, Frick B, Mayorova M, Zorn R (2007) Eur Phys J ST 141:255

61. Donth E (1982) J Non-Cryst Solids 53:325
62. Scheidler P, Kob W, Binder K (2000) J Phys IV 10:33
63. Fakhraai Z, Forrest JA (2005) Phys Rev Lett 95:025701
64. Cicerone MT, Blackburn FR, Ediger MD (1995) Macromolecules 28:8224
65. Kanaya T, Tsukushi I, Kaji K, Bartos J, Kristiak J (2000) J Phys IV France 10:Pr7–Pr317
66. Paratt LG (1954) Phys Rev 95:359
67. Tanaka K, Tateishi Y, Okada Y, Nagamura T, Doi M, Morita H (2009) J Phys Chem B 113:4571
68. Priestley RD, Ellison CJ, Broadbelt LJ, Torkelson JM (2005) Science 309:456
69. Pratt FL, Lancater T, Brooks ML, Blundell SJ, Prokscha T, Morenzoni E, Suter A, Luetkens H, Khasanov R, Scheuermann, Zimmermann U, Shinotsuka K, Assender HE (2005) Phys Rev B 72:121401(R)